CHEMISTRY OF MATERIALS
Cite This: Chem. Mater. 2019, 31, 9024−9031
Article
pubs.acs.org/cm

O_2/O_2^- Crossover- and Dendrite-Free Hybrid Solid-State Na−O_2 Batteries

Xiaoting Lin, Fei Sun, Qian Sun, Sizhe Wang, Jing Luo, Changtai Zhao, Xiaofei Yang, Yang Zhao, Changhong Wang, Ruying Li, and Xueliang Sun*

Department of Mechanical and Materials Engineering, University of Western Ontario, London, Ontario N6A 5B9, Canada

Supporting Information

ABSTRACT: Superoxide-based Na−O_2 batteries have attracted extensive research attention because of their high theoretical energy density and energy efficiency. However, the poor cycling performance caused by O_2/O_2^- crossover and the uncontrollable Na dendrite growth severely hinder their practical applications. Addressing these issues comprehensively, we successfully developed a hybrid solid-state (HSS) Na−O_2 battery based on solid-state electrolyte (SSE) and a protected Na anode. The dense structure of SSE effectively suppressed the O_2/O_2^- crossover, thus mitigating the Na degradation and improving the cell reversibility. Solid electrolyte interphase formation on the Na anode in relation to the O_2/O_2^- crossover was further revealed. Additionally, a three-dimensional protection layer on the Na anode facilitated uniform Na deposition within the conductive matrix. Consequently, the fabricated HSS Na−O_2 battery demonstrated stable cycling for over 160 cycles at 0.2 mA cm^{-2} under the shallow cycling mode. Our results evidently emphasized the critical role of Na anode protection and the importance of O_2/O_2^- blockage for safe and high-performance Na−O_2 batteries.

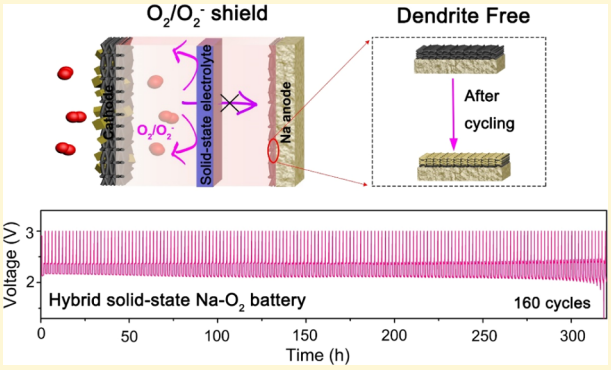

INTRODUCTION

Owing to the appealingly high theoretical energy density, Li−O_2 batteries have been considered as a promising alternative to the state-of-the-art Li-ion batteries.[1−7] However, most Li−O_2 batteries generate insulating Li_2O_2 as the main discharge product, which is a plague on high charging overpotential and thus results in low round-trip energy efficiency.[8−10] Comparatively, Na−O_2 batteries are more favorable for large-scale implementations in terms of high energy efficiency and reversibility.[11−13] In addition, the low cost and abundance of Na on earth promise a long-term future for Na−O_2 batteries in a wide range of applications.[14,15]

Nevertheless, several technical bottlenecks are still limiting the cycle life of Na−O_2 batteries. Especially, O_2 crossover from the air electrode to the Na anode is detrimental for Na−O_2 batteries.[16−20] Parasitic reactions and continuous consumption of the metallic Na anode due to O_2 crossover are one of the main causes of Na−O_2 battery failure.[21,22] Another source of detrimental side reactions on Na metal is induced by the O_2^- migration in superoxide Na−O_2 batteries because of the solution-mediated path for NaO_2 formation.[23−27] In fact, the O_2^- radical is an aggressive species, which is prone to attack electrophilic sites. The effect of O_2^- radicals on promoting parasitic reactions on the Na metal anode is profound despite the relatively low concentration.[28,29] The presence of O_2^- also causes severe decompositions of electrolyte solvents, sodium salts, binders, and air electrodes in superoxide-based Na−O_2 batteries.[30−37] However, studies toward understanding the O_2/O_2^- crossover effect on the nature of solid electrolyte interphase (SEI) and overall cell performance are scarce.

Blocking O_2/O_2^- crossover is of primary importance for enhancing the electrochemical performance of Na−O_2 batteries. In traditional liquid electrolyte (LE)-based Na−O_2 cells with porous separators, the dissolved O_2/O_2^- can diffuse freely from the cathode to the anode. A physical barrier is required to retard the migration of O_2/O_2^-. Inspired by the aqueous Na−air batteries, in which ceramic separators are widely used to prevent the undesirable "cross-talk" of an aqueous electrolyte and organic electrolyte,[38,39] NASICON solid-state electrolyte (SSE) can be an ideal candidate to block the O_2/O_2^- crossover for Na−O_2 batteries. However, the implementation of Na metal anodes in Na−O_2 batteries encounters the Na dendrite formation problem.[40,41] The inhomogeneous current distribution at the Na/NASICON interface inevitably initiates rapid Na dendrite growth along the grain boundaries.[42] The penetration of Na dendrites through the SSE in hybrid solid-state (HSS) Na−O_2 batteries leads to initial short-circuit and safety concerns, especially for aqueous Na−O_2 batteries. While it is still a big challenge to enable both reversible plating/stripping of dendrite-free Na

Received: August 12, 2019
Revised: October 15, 2019
Published: October 16, 2019

DOI: 10.1021/acs.chemmater.9b03266
Chem. Mater. 2019, 31, 9024−9031

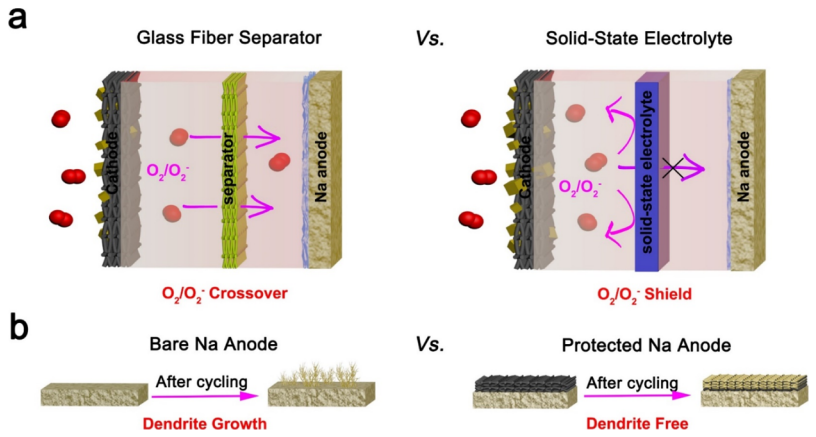

Figure 1. Schematic illustrating the effects of (a) O_2/O_2^- crossover prevention by SSE and (b) dendrite-free Na deposition by anode protection for high-performance HSS Na–O_2 batteries.

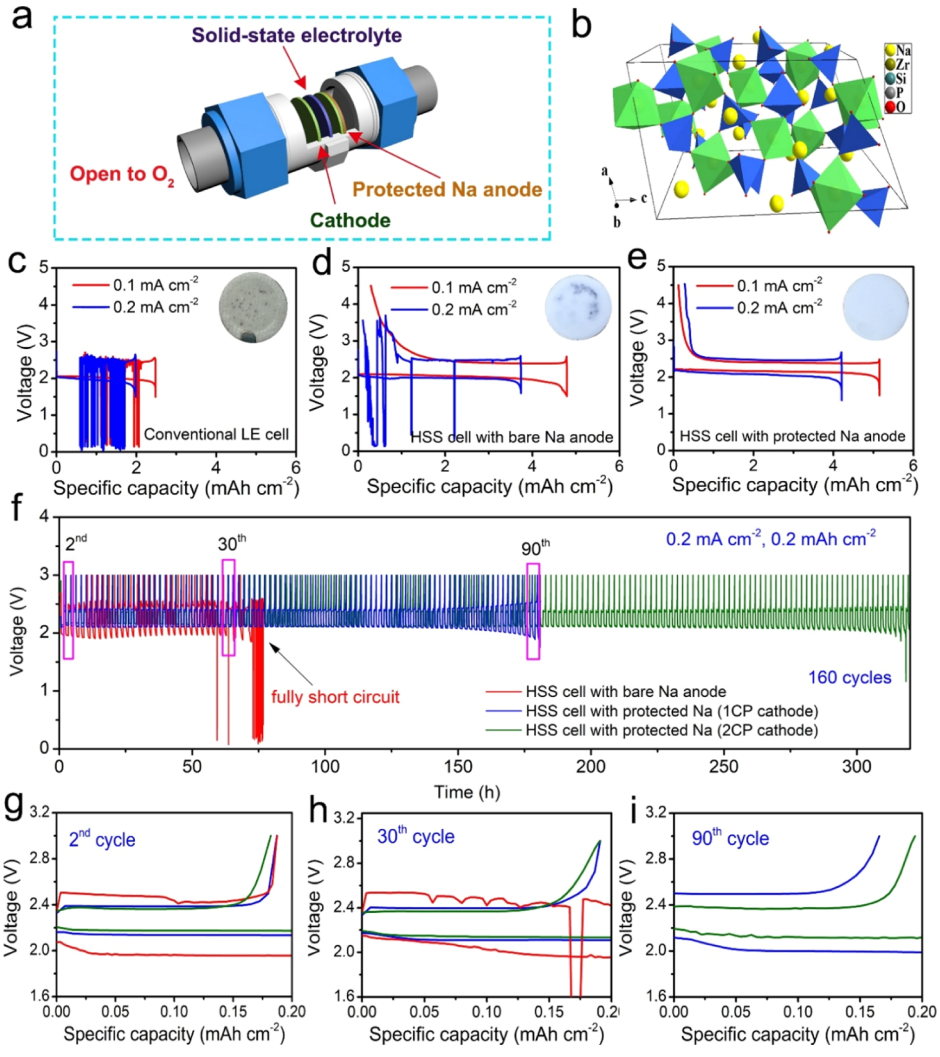

Figure 2. (a) Schematic illustration of a Swagelok-type Na–O_2 cell with SSE and CP-protected Na anode. (b) Crystal structure of NASICON-type NZSPO SSE. The discharge–charge curves of (c) conventional Na–O_2 batteries using LE, (d) HSS cells using NZSPO SSE, and (e) HSS cells using NZSPO SSE and CP-protected Na anode at current densities of 0.1 and 0.2 mA cm^{-2}; the insets are corresponding optical images of the separator or SSE collected after fully recharged at 0.2 mA cm^{-2}; (f) cycling performance of HSS Na–O_2 batteries with or without CP protection on the Na anode at 0.2 mA cm^{-2} with a limited capacity of 0.2 mA h cm^{-2}; (g–i) charge–discharge voltage profiles at the 2nd, 30th, and 90th cycles [profile colors are as labeled in (f)].

anodes and O_2/O_2^- blockage simply with the NASICON pellet, the combination of SSE together with a protected Na anode could be a promising strategy to achieve high efficiency and long life Na–O_2 batteries.

DOI: 10.1021/acs.chemmater.9b03266
Chem. Mater. 2019, 31, 9024–9031

In this work, we successfully demonstrate a high-performance HSS Na−O_2 battery with effective O_2/O_2^- crossover prevention and dendrite-free Na metal protection. Unlike the Na−O_2 batteries with LE and a porous glass fiber (GF) separator, the dense structure of NASICON SSE is Na^+ conductive but impermeable to O_2/O_2^-, effectively avoiding Na metal corrosion and enhancing the reversible capacity. Furthermore, commercial carbon paper (CP) can be used not only as the air electrode directly but also as the versatile dendrite-free protector for the Na metal anode (Figure 1b). The additional CP between SSE and the Na metal anode facilitates dendrite-free deposition of Na within the three-dimensional (3D) framework. Owing to the combined advantages of SSE and CP modification, the developed HSS Na−O_2 cell delivered high discharge capacities with excellent Coulombic efficiency (CE) as well as stable cycling performance.

EXPERIMENTAL SECTION

Material Synthesis. The SSE $Na_{3.25}Zr_2Si_{2.25}P_{0.75}O_{12}$ was synthesized via a sol−gel method. Stoichiometric amounts of tetraethyl orthosilicate ($Si(OC_2H_5)_4$, TEOS) (Sigma-Aldrich, 98%) and zirconium(IV) propoxide solution ($Zr(OC_4H_9)_4$) (Sigma-Aldrich, 99.99%) were sequentially dissolved in ethanol. Then, acetic acid and deionized water were added into the mixture dropwise, and the mixture sol was kept at 67 °C under vigorous stirring for 10 h. Then, the sodium nitrate (Sigma-Aldrich, 99.0%) and ammonium dihydrogen phosphate (Prolabo, 99.9%) were, respectively, dissolved in water, and the solution was successively added into the hot mixture of silica and zirconia. In the next step, the solution was slowly evaporated at 67 °C to produce the precursor powder with stirring, which was then heated at 500 °C for 1 h under the O_2 atmosphere to burn out the organics. After this, the obtained powder was annealed at 1050 °C for 10 h and then uniaxially pressed into pellets, which were sintered at 1300 °C for 12 h in the air atmosphere.

Materials. The CP (Freudenberg H23, thickness of 210 μm), purchased from Fuel Cell Store, was utilized as the cathode and anode protector in the Na−O_2 batteries after drying in vacuum at 80 °C for 3 days. Diethylene glycol dimethyl ether (DEGDME, reagent grade ≥98%, Aldrich) was dried over freshly activated molecular sieves (4 Å, Aldrich) for at least 1 month. Sodium trifluoromethanesulfonate ($NaSO_3CF_3$, Aldrich) was dried in vacuum at 80 °C for 3 days before use.

Characterizations. The powder X-ray diffraction (XRD) patterns were analyzed on the Bruker D8 X-ray diffractometer equipped with Cu Kα (λ = 1.5406 Å) radiation. The morphology of the cathodes after discharge was characterized by a Hitachi S-4800 field emission scanning electron microscope, and the morphological studies of the CP interlayer were determined using a Hitachi 3400N environmental scanning electron microscope. The Raman spectra were collected on a HORIBA Scientific LabRAM Raman spectrometer equipped with a 532.03 nm laser. In this study, the disassembly of the Na−O_2 batteries was carried out in an ultrapure argon-filled glovebox. The discharged cathodes were washed with fresh DEGDME to remove any residual $NaSO_3CF_3$ salt and then rigorously dried in the vacuum chamber before scanning electron microscopy (SEM), XRD, and Raman measurements. The dried samples were sealed into a leak-tight homemade sample holder to prevent the exposure of air during sample testing.

Electrochemical Characterizations. The ionic conductivity of the $Na_{3.25}Zr_2Si_{2.25}P_{0.75}O_{12}$ pellet was measured through electrochemical impedance spectroscopy (EIS) using Au film sputtered on both sides of the pellet as blocking electrodes, and EIS was performed over a frequency range of 1 MHz to 100 mHz with a 50 mV perturbation amplitude. The electrochemical performance of Na−O_2 batteries was evaluated with Swagelok-type cells. The HSS Na−O_2 batteries were assembled with the Na metal anode, $Na_{3.25}Zr_2Si_{2.25}P_{0.75}O_{12}$ SSE, CP cathode, and ether electrolyte. The CP cathode and Na metal foil were cut into circular pieces with a geometric surface area of 0.7125 cm^{-2}. The electrolyte was 0.5 M $NaSO_3CF_3$ dissolved in DEGDME. A minor amount of LE (2 μL) was added on the Na anode to mitigate the poor SSE/Na interfacial contact and, at the same time, facilitate the ion conduction during the cell cycling process. While on the cathode side, 30 μL of LE was added to facilitate the formation of NaO_2 through a solution-mediated path. The cells were operated under static O_2 with the pressure of 1.0 atm in a homemade testing box, and each cell was stabilized for 30 min at room temperature before electrochemical tests. The galvanostatic discharge−charge tests were carried out using an Arbin BT-2000 battery testing system at room temperature. The electrochemical analysis of Na symmetric cells was performed using CR2032 coin-type cells. The electrolyte preparation and battery assembly were carried out in an argon-filled glovebox with the oxygen and moisture levels below 0.1 ppm.

RESULTS AND DISCUSSION

Figure 2a schematically illustrates the configuration of the designed HSS Na−O_2 battery. Commercial CP was used as the cathode; NASICON-type $Na_{3.25}Zr_2Si_{2.25}P_{0.75}O_{12}$ (NZSPO) was used as the electrolyte and separator; and another layer of LE-infiltrated CP was placed on the Na metal for a dendrite-free anode. Here, NZSPO was chosen in this work because of its high ionic conductivity, wide electrochemical stability window, as well as good stability against Na metal (Figures S1and S2). NZSPO powder was synthesized by a modified sol−gel synthesis-combustion method and subsequently sintered and polished into thin SSE pellets.[43] The structure of NZSPO SSE is shown in Figure 2b. XRD pattern of the synthesized NZSPO confirmed its desired phase (Figure S3).[44]

As a proof of concept, the electrochemical performance of the proposed HSS Na−O_2 cells with NZSPO SSE and CP-protected Na anode was tested in a potential range of 1.5−4.5 V. Meanwhile, Na−O_2 cells using conventional LE with GF separator as well as HSS Na−O_2 cells using bare Na anode were assembled for comparison. As shown in Figure 2c, the conventional LE cells with the GF separator delivered low initial discharge capacities of 2.48 and 1.98 mA h cm^{-2} at 0.1 and 0.2 mA cm^{-2}, respectively. The worst thing was that the LE Na−O_2 cells failed to be recharged because Na dendrites induced short-circuit.[21,45] Na dendrite dead spots were clearly observed in the optical image of the GF separator collected after cell failure (inset in Figure 2c). Noticeably, replacing the GF separator with dense NZSPO SSE significantly increased the initial discharge capacities of the Na−O_2 cells to 4.8 and 3.7 mA h cm^{-2} at 0.1 and 0.2 mA cm^{-2}, respectively (Figure 2d). Upon recharging, the HSS Na−O2 cell with bare Na anode can be charged at 0.1 mA cm^{-2} with an adequate CE of 93.8%. However, the HSS Na−O_2 cell with bare Na anode still encountered short-circuit at a current density of 0.2 mA cm^{-2} because of the accelerated Na dendrite growth during charging (inset in Figure 2d). The implementation of NZSPO SSE enhanced the electrochemical performance of Na−O_2 cells to some extent but not yet to the practical level. Efforts to further address the Na dendrite formation issue in HSS Na−O_2 batteries are required.

Taking the advantage of CP as a 3D electronic conductive matrix to accommodate Na deposition, HSS Na−O_2 cells utilizing NZSPO SSE and CP-protected Na anode demonstrated significantly improved electrochemical performance. High initial discharge capacities of 5.15 and 4.21 mA h cm^{-2} were delivered at 0.1 and 0.2 mA cm^{-2}, respectively, which were more than twice the LE cell (Figure 2e). Moreover, the

DOI: 10.1021/acs.chemmater.9b03266
Chem. Mater. 2019, 31, 9024−9031

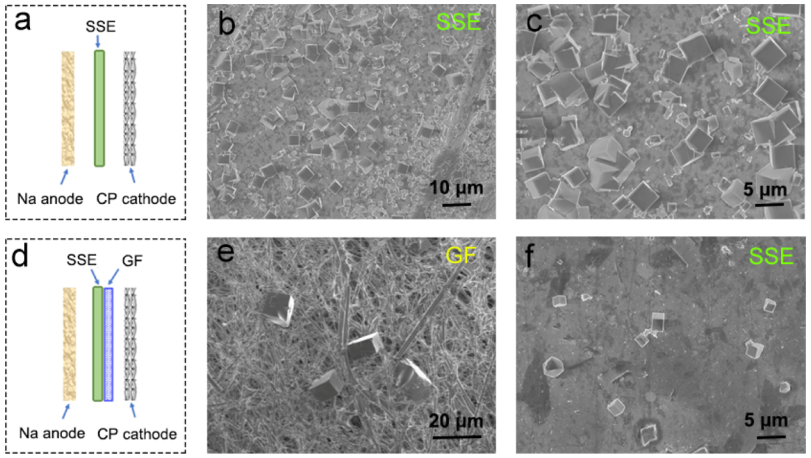

Figure 3. (a) Schematic diagram of the HSS Na−O_2 cell with SSE and (b,c) corresponding SEM images of the SSE surface (cathode side) after discharging for 50 h at 0.1 mA cm^{-2}. (d) Schematic diagram of the HSS Na−O_2 cell with SSE and additional GF separator; corresponding SEM images of (e) GF and (f) SSE after discharging for 50 h at 0.1 mA cm^{-2}.

introduction of SSE can significantly decrease the reversible charge capacity loss, and thus, high CEs of 97.6 and 93.5% can be achieved at 0.1 and 0.2 mA cm^{-2}, respectively. It should be noted that these CEs are higher than that of the LE cells with the protected Na anode in our previous report.[24] The SSE obviously played important roles in enhancing the discharge capacities and improving the reversibility of the Na−O_2 cells. Moreover, after disassembling the fully recharged cell, the surface of the SSE remained unchanged without observable dark dendrite spots (inset in Figure 2e). The LE-infiltrated soft CP layer can compensate the roughness of the SSE/Na interface and facilitate even ion flux, and the 3D CP matrix provided buffer for accommodating dendrite-free Na deposition (Figure S4).[24] The effectiveness of Na anode protection in preventing the dendrite-induced short-circuit was also demonstrated by the extended cycle life and stable voltage profiles of Na symmetric cells (Figures S5and S6). Note that similar initial spike of potential during the charge process can be clearly observed for three types of Na−O_2 cells despite the distinct discharge−charge behaviors (Figure 2c−e). The initial increase of charge overpotential can be correlated to the formation of carbonate-based side products at the outer shell of the NaO_2 cube because of the instability of the organic electrolyte, which acts as an initial barrier for the reversible decomposition of NaO_2.[46,47]

To further validate the synergistic effect of SSE and the protected Na anode, long-term cycling performance of LE and HSS Na−O_2 cells was compared at 0.2 mA cm^{-2} with a cutoff capacity of 0.2 mA h cm^{-2} (Figure 2f). Using one layer of CP (1CP) as the cathode, the HSS Na−O_2 cell with the protected Na anode maintained stable cycling for over 90 cycles with a high CE, whereas the charge voltage of the HSS Na−O_2 cell with bare Na encountered sudden drops because of the dendrite penetration and failed to cycle beyond 35 times. The Na dendrite growth problem was even more severe in the LE cell, which soon experienced dendrite-induced short-circuit at the 19th cycle (Figure S7). The CP modification on the Na anode played an effective role in preventing the cell short-circuit and extending the cycle life of HSS Na−O_2 cells. In addition, the conductive CP modification on the Na anode significantly reduced the discharge−charge overpotential of the Na−O_2 cell (Figure 2g,h). The discharge−charge voltage profile of the LE Na−O_2 cell was subjected to continuously enlarging polarization, presumably because of Na degradation by O_2/O_2^- crossover (Figure S7).[24] In contrast, the voltage profiles of the HSS Na−O_2 batteries with the CP-protected Na anode remained stable over the cycling duration (Figure 2f), indicating unchanged internal resistance.

In addition to the dendrite-induced short-circuit and Na anode degradation, insufficient cathode can be another limiting factor for the Na−O_2 cycle life. To further clarify the origin failure for the HSS Na−O_2 cell with the protected Na anode, another cell with extra cathode loading [two layers of CP (2CP) instead of 1CP as the cathode] was tested. Interestingly, we found that the cell with the 2CP cathode actually significantly extended the cycle life to over 160 cycles with stable performance (Figure 2f), compared with 90 cycles for the cell with the 1CP cathode. Evidently, it was the cathode (CP) rather than the anode (protected Na) that limited the cycle life of Na−O_2 batteries. By investigating the morphological changes of the CP cathode at different cycles, it can be clearly observed that the surface of the air electrode was gradually covered by side products upon cycling (Figure S8). We can conclude that the gradual shielding of active sites by accumulated side products can be the intermediate cause of the increased discharge−charge overpotentials after 70 cycles and the limited cycle life of the Na−O_2 cell with the 1CP cathode (Figure 2f–i). Presumably, the decomposition of the ether electrolyte against superoxides and the reaction between the CP cathode and reactive discharge product(s) led to the formation of side products.[22,46] Note that the constructed HSS Na−O_2 cells exhibit one of the best electrochemical performances among all the superoxide-based Na−O_2 batteries that use the same CP cathode (Table S1). It can be expected that the cycle life of HSS Na−O_2 cells with the protected Na anode can further achieve even longer cycle life using an advanced air electrode.[4]

The chemical composition and morphology of the discharge product at the cathode of the HSS Na−O_2 cell were characterized at the fully discharged state at 0.1 mA cm^{-2}. As shown in Figure S9, the discharge product of the HSS Na−O_2 cell was typical cubic-shaped NaO_2 based on SEM, XRD, and Raman characterizations. The morphological evolution of the discharge product (NaO_2) in the HSS Na−O_2 cells was further explored at different discharge capacities, as shown in Figure S10. A few NaO_2 cubes and many discreet nuclei were

DOI: 10.1021/acs.chemmater.9b03266
Chem. Mater. 2019, 31, 9024−9031

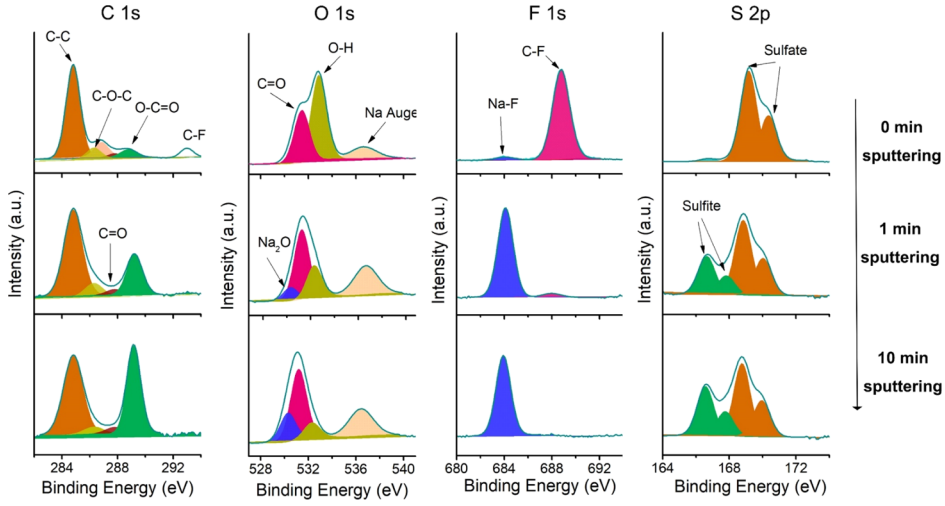

Figure 4. XPS characterization of the Na anode SEI layer formed in the LE Na−O_2 cell in the presence of O_2/O_2^- crossover.

observed on the carbon fiber surface at a low discharge capacity of 0.2 mA h cm^{-2} (Figure S10a,b). When the cell was discharged to 0.5 mA h cm^{-2}, the discreet nuclei evolved into cubic-shaped particles and, at the same time, new NaO_2 nuclei precipitate on the surface of carbon fibers. This process proceeded with increasing discharge capacity, thus increasing the size and density of the NaO_2 cubes (Figure S10c,d). At a large discharge capacity of 3 mA h cm^{-2}, the neighboring NaO_2 cubes merged and gradually covered up the carbon fiber surface (Figure S10e). The oxygen reduction reaction of the HSS Na−O_2 cell terminates when the pores on the oxygen side of the air electrode were fully blocked, which is known as the pore-clogging effect (Figure S10f).

The solution-based mechanism for the formation of NaO_2 in Na−O_2 batteries has been widely accepted, and it has been reported that the Na metal in the cell environment directly or indirectly contributed to the migration of O_2^- from the cathode to the anode.[23] To demonstrate the effect of SSE in blocking the crossover of O_2^-, the morphological characterization of the SSE in different cell configurations was conducted (Figure 3). The NZSPO SSE pellet has a dense structure without obvious pores (Figure S11). After the HSS Na−O_2 cell was discharged for 50 h at 0.1 mA cm^{-2}, numerous NaO_2 cubes sized approximately 1−5 μm were deposited on the SSE surface toward the air electrode (Figures 3b,c and S12). The randomly distributed indentations were due to the attachment of carbon fibers on the SSE (Figure 3b). Because electrochemical reactions require access to both Na^+ ions and electrons, the electrochemical formation of NaO_2 would not occur on the insulating GF by definition. With an additional piece of GF separator placed between SSE and the cathode (Figure 3d), we can distinguish the diffusion products from the reaction products. Corresponding SEM images of the GF separator and the SSE obtained at the fully discharged state are shown in Figures 3e,f and S13. Interestingly, crystalline NaO_2 was observed on the surface of both the GF and SSE. These NaO_2 cubes were diffusion products from the CP cathode. The GF separator and LE are obviously permeable to the dissolved O_2^- intermediate, leading to O_2^- crossover.

Taking a closer look into the NaO_2 products at different locations, their morphologies were actually significantly different. The NaO_2 cubes on the GF separator were as large as 20 μm, while a few discrete NaO_2 cubes with a much smaller size (~2 μm) were observed on SSE, which also differed from the NaO_2 cubes observed on the SSE without GF separation. This can be explained by the concentration difference of the O_2^-−Na^+ species in the organic electrolyte as well as the rate of nucleation and diffusion of $(O_2^-{-}Na^+)_n$ onto SSE versus GF separator. When the CP cathode was in direct contact with the SSE in the HSS Na−O_2 cell (Figure 3a), the concentration of the soluble O_2^-−Na^+ could quickly build up on the SSE surface as the dense structure of SSE terminated the passage of the O_2^- species, while the interface with CP was still accessible to electrons. The high nucleation rate led to a high concentration of NaO_2 nuclei at the SSE/CP interface, where the NaO_2 nuclei grew larger in size upon increasing discharge capacities. In the other cell configuration with an extra GF layer, the O_2^- concentration at the cathode side of the GF separator precedently reached saturation and initiated the nucleation of NaO_2 on GF. Subsequently, the soluble O_2^- anions diffused across the GF layer under dual effects of ion concentration gradient and electric field. Therefore, the NaO_2 nucleation kinetics on GF was low; at the same time, continuous growth of NaO_2 particulates occurred preferentially at the existing NaO_2 nuclei. The resulting NaO_2 particles on GF were thus scattered and large in size. On the other hand, the precipitation of NaO_2 on the GF separator still diluted the amount of NaO_2 accumulation on the SSE. This explains the observation of less NaO_2 cubes with smaller size on the SSE compared with that of the HSS Na−O_2 cell in Figure 3c. Note that NaO_2 cubes cannot be observed on the SSE surface toward the negative electrode because of the shielding effect of SSE toward O_2^- crossover.

In addition to the O_2^- crossover suppressing the characteristic of the SSE, its chemical stability against the highly reactive NaO_2 is also very important for high-performance HSS Na−O_2 batteries. While the apparent accumulation of NaO_2 on the SSE readily proofed their stability with each other, XRD and Raman characterizations were also conducted before and after the full recharge of the HSE Na−O_2 cells at 0.1 mA cm^{-2} to confirm. The NZSPO phase was well maintained after cycling, indicating the excellent chemical stability of the SSE toward the highly oxidative NaO_2 (Figure S14).

However, as a strong oxidant, O_2^- can easily react with the Na anode, resulting in continuous O_2^- crossover and serious Na degradation.[23] To systematically elucidate the O_2/O_2^-

DOI: 10.1021/acs.chemmater.9b03266
Chem. Mater. 2019, 31, 9024−9031

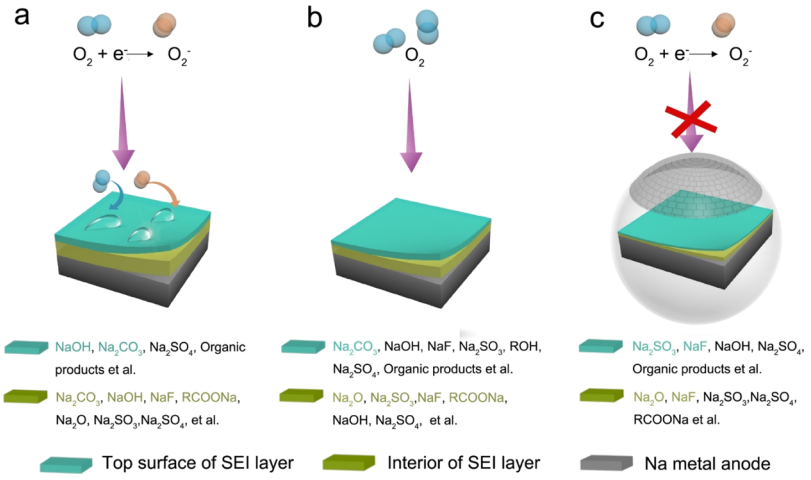

Figure 5. Schematic illustration of the SEI formation on the Na metal surface in the presence of (a) O_2/O_2^- crossover and (b) O_2 crossover and in the absence of (c) O_2/O_2^- crossover.

crossover-induced Na degradation mechanism, X-ray photoelectron spectroscopy (XPS) analyses with depth profiling were conducted on the Na metal anode. The LE Na−O_2 cell with a porous separator was disassembled after discharging for 12 h at 0.1 mA cm^{-2} to examine the SEI compositions on the Na anode surface. Figure 4 shows the XPS spectra of C 1s, O 1s, S 2p, and F 1s. At 0 min of sputtering, the peaks at 284.8, 286.7, and 288.8 eV in the C 1s spectrum can be assigned to the presence of C−C/C−H, C−O, and O−C═O, respectively, as a result of DEGDME solvent decomposition.[48] At the same time, the O 1s spectrum shows the characteristic peaks of Na_2CO_3 and NaOH at 531.3 and 532.8 eV, respectively.[21] The F 1s feature at 688.7 eV (C−F) and the S $2p_{3/2}$ peak at 168.6 eV (SO_4^{2-}) were likely resulted from the decomposition of the $NaSO_3CF_3$ salt. Combining these information, we can deduce that the top surface of the anode SEI film is mainly composed of inorganic (NaOH, Na_2CO_3, and Na_2SO_4) and organic (RCOONa, CF_x, etc.) components for the discharged LE Na−O_2 cell. After 1 min of sputtering, the O, F, and S peaks corresponding to inorganic Na_2O (530.9 eV), NaF (683.8 eV), and Na_2SO_3 (166.6 and 167.7 eV) emerged and remained distinct after 10 min of sputtering. Meanwhile, the O−C═O peak corresponding to the organic reduction product ROCOONa became stronger after 10 min of sputtering, suggesting a higher content in the depth. Overall, the SEI layer is composed of both organic and inorganic components across the depth from the top surface to the interior, with a changing composition. Notably, Na_2CO_3 contributed to a large proportion across the depth of the SEI layer; the NaOH component also penetrated throughout the SEI layer but showed a reducing amount toward the interior.

To distinguish between the effects of O_2 versus O_2^- crossovers, another LE Na−O_2 cell was allowed to rest in an O_2 atmosphere for 12 h without discharging. In this case, NaO_2 was not generated, so the SEI formation on the Na anode surface was mainly affected by the O_2 crossover in the absence of O_2^-. As shown in Figure S15, the evolution of RCOONa, Na_2O, NaF, NaOH, and sulfate compositions in the SEI was consistent with those in the SEI of the discharged LE Na−O_2 cell. The SEI also contained both the organic and inorganic components. However, the relative concentration of NaOH and Na_2CO_3 on the top surface of the SEI layers varied in two cases. In the presence of both O_2 and O_2^-, the NaOH component rather than Na_2CO_3 dominated the superficial SEI; however, the Na_2CO_3 component was more pronounced in the case of only O_2 crossover. Additionally, different from the case of the discharged SEI in which the NaF and sulfite were not observable at 0 min of sputtering, characteristic XPS peaks for sulfite and NaF species were clearly observed on the top SEI surface when formed at rest with O_2, indicating a relatively thinner top SEI surface.

In fact, the anode SEI layer of the HSS Na−O_2 cell was distinct from the LE cell when the O_2/O_2^- crossover was inhibited (Figure S16). At 0 min of sputtering, the peak corresponding to NaF as well as the peaks for sulfite species was observed. After sputtering for 1 and 10 min, the peaks for NaOH and Na_2CO_3 essentially faded, while the Na_2O and NaF peaks became the dominating feature in the interior SEI. The interior SEI composition was particularly favorable as the protective inorganic SEI layer for the Na anode. In addition, the weaker peak intensities of the S 2p and F 1s spectra may indicate less decomposition of $NaSO_3CF_3$ in the HSS Na−O_2 cell compared with that in the LE Na−O_2 cell.

By comparison, with or without O_2 and/or O_2^- crossovers, a significant difference was made in the Na anode SEI formation in Na−O_2 battery systems (Figure 5). Similar to Li−O_2 and K−O_2 batteries, the crossover of O_2 in the Na−O_2 batteries also contributes to the decomposition of the electrolyte and the subsequent formation of NaOH and Na_2CO_3 on the Na anode. Compared to O_2, the highly reactive O_2^- can induce intensified side reactions, causing not only corrosion of the Na metal anode but also severe decomposition of the electrolyte. As an evidence, the SO_4^{2-} species on the top surface of the SEI layer may be resulted from the further oxidation of SO_3^{2-} by the crossover of O_2/O_2^-, while some SO_3^{2-} still remained in the interior SEI. Moreover, the presence of organic products throughout the anode SEI layer in the LE Na−O_2 cell can lead to a loose SEI structure (Figure 5a,b), which is permeable to O_2/O_2^- and electrolyte. Hence, the electrolyte decomposition and SEI layer growth could occur continuously. The consequent increase of cell internal resistance can deteriorate the cell performance. We postulate that the restricted performances and the premature cell death of LE Na−O_2 cells arise from the crossover of O_2/O_2^-. However, by implementing the SSE, the O_2/O_2^- crossover can be inhibited along with the formation of an inorganic NaF protective layer

DOI: 10.1021/acs.chemmater.9b03266
Chem. Mater. 2019, 31, 9024−9031

(Figures 5c and S15). This could be a reason for the stable charge−discharge overpotential of the HSS Na−O_2 cell when the cathode was sufficient (Figure 2f). Therefore, controlling the O_2/O_2^- crossover to the Na anode surface by a highly stable SSE can be an effective strategy for achieving good performance of superoxide-based Na−O_2 batteries.

CONCLUSIONS

In summary, we successfully constructed a HSS Na−O_2 battery free of Na dendrites and oxygen species crossover by coupling a NASICON SSE and a protected Na anode. The SSE functions as a shield to the O_2/O_2^- migrations and eliminates detrimental side reactions on the Na anode surface. The CP-modified Na anode complementarily addressed the Na dendrite growth issues. Moreover, the SEI formation on the Na anode in relation to O_2/O_2^- crossover is systematically analyzed by XPS with the depth profile, revealing a favorable NaF-rich inorganic SEI enabled by the SSE shielding of O_2/O_2^-. Although more future work will be needed to make the Na−O_2 battery system commercially viable, the results presented here provide valuable guidance for fabricating advanced Na−O_2 batteries with longer life spans and better cycling performance.

ASSOCIATED CONTENT

Supporting Information

The Supporting Information is available free of charge on the ACS Publications website at DOI: 10.1021/acs.chemmater.9b03266.

SEM images of the discharged CP cathode, XRD patterns and Raman spectra of discharge products, additional sample electrochemical performance characterization, and XPS spectra (PDF)

AUTHOR INFORMATION

Corresponding Author

*E-mail: xsun9@uwo.ca.

ORCID

Xueliang Sun: 0000-0003-0374-1245

Author Contributions

X.L. and F.S. contributed equally to this work. X.L. and Q.S. designed the experimental work with the help from Y.Z. who proposed method for Na protection; S.W. and X.Y. helped with the schematic diagram; C.W. performed the XRD characterization; X.L., Q.S., C.Z., and J.L. participated in the discussion of the data; X.S. supervised the overall project. All authors have given approval to the final version of the manuscript.

Notes

The authors declare no competing financial interest.

ACKNOWLEDGMENTS

This research was supported by National Sciences and Engineering Research Council of Canada, Canada Research Chair Program, Canada Foundation for Innovation, the Ontario Research Fund, and the University of Western Ontario. X.L. was supported by the Chinese Scholarship Council.

REFERENCES

(1) Peng, Z.; Freunberger, S. A.; Chen, Y.; Bruce, P. G. A Reversible and Higher-Rate Li-O_2 Battery. *Science* **2012**, *337*, 563−566.

(2) Lu, J.; Lei, Y.; Lau, K. C.; Luo, X.; Du, P.; Wen, J.; Assary, R. S.; Das, U.; Miller, D. J.; Elam, J. W.; Albishri, H. M.; El-Hady, D. A.; Sun, Y.-K.; Curtiss, L. A.; Amine, K. A nanostructured cathode architecture for low charge overpotential in lithium-oxygen batteries. *Nat. Commun.* **2013**, *4*, 2383.

(3) Khajehbashi, S. M. B.; Li, J.; Wang, M.; Xu, L.; Zhao, K.; Wei, Q.; Shi, C.; Tang, C.; Huang, L.; Wang, Z.; Mai, L. A Crystalline/Amorphous Cobalt(II,III) Oxide Hybrid Electrocatalyst for Lithium−Air Batteries. *Energy Technol.* **2017**, *5*, 568−579.

(4) Jian, Z.; Liu, P.; Li, F.; He, P.; Guo, X.; Chen, M.; Zhou, H. Core−Shell-Structured CNT@RuO_2 Composite as a High-Performance Cathode Catalyst for Rechargeable Li−O_2 Batteries. *Angew. Chem., Int. Ed.* **2014**, *53*, 442−446.

(5) Wang, Y.-J.; Yuan, R.; Ignaszak, A.; Wilkinson, D. P.; Zhang, J.; Ignaszak, A.; Zhang, L.; Zhang, J. A Review of Carbon-Composited Materials as Air-Electrode Bifunctional Electrocatalysts for Metal−Air Batteries. *Advanced Bifunctional Electrochemical Catalysts for Metal−Air Batteries*, 2018; CRC Press; Vol. *1*, pp 1−34.

(6) Bruce, P. G.; Freunberger, S. A.; Hardwick, L. J.; Tarascon, J.-M. Li-O_2 and Li-S batteries with high energy storage. *Nat. Mater.* **2012**, *11*, 19−29.

(7) Wei, Q.; Tan, S.; Liu, X.; Yan, M.; Wang, F.; Li, Q.; An, Q.; Sun, R.; Zhao, K.; Wu, H.; Mai, L. Novel Polygonal Vanadium Oxide Nanoscrolls as Stable Cathode for Lithium Storage. *Adv. Funct. Mater.* **2015**, *25*, 1773−1779.

(8) Yadegari, H.; Norouzi Banis, M.; Lushington, A.; Sun, Q.; Li, R.; Sham, T.-K.; Sun, X. A bifunctional solid state catalyst with enhanced cycling stability for Na and Li−O_2 cells: revealing the role of solid state catalysts. *Energy Environ. Sci.* **2017**, *10*, 286−295.

(9) Zhao, C.; Yu, C.; Banis, M. N.; Sun, Q.; Zhang, M.; Li, X.; Liu, Y.; Zhao, Y.; Huang, H.; Li, S.; Han, X.; Xiao, B.; Song, Z.; Li, R.; Qiu, J.; Sun, X. Decoupling atomic-layer-deposition ultrafine RuO_2 for high-efficiency and ultralong-life Li-O_2 batteries. *Nano Energy* **2017**, *34*, 399−407.

(10) Zhang, Y.; Li, X.; Zhang, M.; Liao, S.; Dong, P.; Xiao, J.; Zhang, Y.; Zeng, X. IrO_2 nanoparticles highly dispersed on nitrogen-doped carbon nanotubes as an efficient cathode catalyst for high-performance Li-O_2 batteries. *Ceram. Int.* **2017**, *43*, 14082−14089.

(11) Hartmann, P.; Bender, C. L.; Vračar, M.; Dürr, A. K.; Garsuch, A.; Janek, J.; Adelhelm, P. A rechargeable room-temperature sodium superoxide (NaO_2) battery. *Nat. Mater.* **2013**, *12*, 228−232.

(12) Sun, B.; Katja, K.; Xiuqiang, X.; Paul, M.; Zhangquan, P.; Guoxiu, W. Hierarchical Porous Carbon Spheres for High-Performance Na−O_2 Batteries. *Adv. Mater.* **2017**, *29*, 1606816.

(13) Bender, C. L.; Hartmann, P.; Vračar, M.; Adelhelm, P.; Janek, J. On the Thermodynamics, the Role of the Carbon Cathode, and the Cycle Life of the Sodium Superoxide (NaO_2) Battery. *Adv. Energy Mater.* **2014**, *4*, 1301863.

(14) Yadegari, H.; Sun, Q.; Sun, X. Sodium-Oxygen Batteries: A Comparative Review from Chemical and Electrochemical Fundamentals to Future Perspective. *Adv. Mater.* **2016**, *28*, 7065−7093.

(15) Yadegari, H.; Sun, X. Recent Advances on Sodium−Oxygen Batteries: A Chemical Perspective. *Acc. Chem. Res.* **2018**, *51*, 1532−1540.

(16) Assary, R. S.; Lu, J.; Du, P.; Luo, X.; Zhang, X.; Ren, Y.; Curtiss, L. A.; Amine, K. The Effect of Oxygen Crossover on the Anode of a Li−O_2 Battery using an Ether-Based Solvent: Insights from Experimental and Computational Studies. *ChemSusChem* **2013**, *6*, 51−55.

(17) Shui, J.-L.; Okasinski, J. S.; Kenesei, P.; Dobbs, H. A.; Zhao, D.; Almer, J. D.; Liu, D.-J. Reversibility of anodic lithium in rechargeable lithium−oxygen batteries. *Nat. Commun.* **2013**, *4*, 2255.

(18) Ren, X.; Lau, K. C.; Yu, M.; Bi, X.; Kreidler, E.; Curtiss, L. A.; Wu, Y. Understanding Side Reactions in K−O_2 Batteries for Improved Cycle Life. *ACS Appl. Mater. Interfaces* **2014**, *6*, 19299−19307.

DOI: 10.1021/acs.chemmater.9b03266
Chem. Mater. 2019, 31, 9024−9031

(19) Marinaro, M.; Balasubramanian, P.; Gucciardi, E.; Theil, S.; Jörissen, L.; Wohlfahrt-Mehrens, M. Importance of Reaction Kinetics and Oxygen Crossover in aprotic Li−O_2 Batteries Based on a Dimethyl Sulfoxide Electrolyte. *ChemSusChem* **2015**, *8*, 3139−3145.
(20) Kraytsberg, A.; Ein-Eli, Y. Review on Li-air batteries–opportunities, limitations and perspective. *J. Power Sources* **2011**, *196*, 886.
(21) Bi, X.; Ren, X.; Huang, Z.; Yu, M.; Kreidler, E.; Wu, Y. Investigating dendrites and side reactions in sodium-oxygen batteries for improved cycle lives. *Chem. Commun.* **2015**, *51*, 7665−7668.
(22) Wu, S.; Qiao, Y.; Jiang, K.; He, Y.; Guo, S.; Zhou, H. Tailoring Sodium Anodes for Stable Sodium−Oxygen Batteries. *Adv. Funct. Mater.* **2018**, *28*, 1706374.
(23) Liu, C.; Carboni, M.; Brant, W. R.; Pan, R.; Hedman, J.; Zhu, J.; Gustafsson, T.; Younesi, R. On the Stability of NaO_2 in Na−O_2 Batteries. *ACS Appl. Mater. Interfaces* **2018**, *10*, 13534−13541.
(24) Lin, X.; Qian, S.; Hossein, Y.; Xiaofei, Y.; Yang, Z.; Changhong, W.; Jianneng, L.; Alicia, K.; Ruying, L.; Xueliang, S. On the Cycling Performance of Na-O_2 Cells: Revealing the Impact of the Superoxide Crossover toward the Metallic Na Electrode. *Adv. Funct. Mater.* **2018**, *28*, 1801904.
(25) Xia, C.; Black, R.; Fernandes, R.; Adams, B.; Nazar, L. F. The critical role of phase-transfer catalysis in aprotic sodium oxygen batteries. *Nat. Chem.* **2015**, *7*, 496−501.
(26) Xia, C.; Fernandes, R.; Cho, F. H.; Sudhakar, N.; Buonacorsi, B.; Walker, S.; Xu, M.; Baugh, J.; Nazar, L. F. Direct Evidence of Solution-Mediated Superoxide Transport and Organic Radical Formation in Sodium-Oxygen Batteries. *J. Am. Chem. Soc.* **2016**, *138*, 11219−11226.
(27) Ma, S.; McKee, W. C.; Wang, J.; Guo, L.; Jansen, M.; Xu, Y.; Peng, Z. Mechanistic origin of low polarization in aprotic Na-O_2 batteries. *Phys. Chem. Chem. Phys.* **2017**, *19*, 12375−12383.
(28) Lee, H.; Lee, D. J.; Lee, J.-N.; Song, J.; Lee, Y.; Ryou, M.-H.; Park, J.-K.; Lee, Y. M. Chemical aspect of oxygen dissolved in a dimethyl sulfoxide-based electrolyte on lithium metal. *Electrochim. Acta* **2014**, *123*, 419−425.
(29) Li, N.; Xu, D.; Bao, D.; Ma, J.; Zhang, X. A binder-free, flexible cathode for rechargeable Na-O_2 batteries. *Chin. J. Catal.* **2016**, *37*, 1172−1179.
(30) Zhao, N.; Guo, X. Cell Chemistry of Sodium−Oxygen Batteries with Various Nonaqueous Electrolytes. *J. Phys. Chem. C* **2015**, *119*, 25319−25326.
(31) Kim, J.; Lim, H.-D.; Gwon, H.; Kang, K. Sodium-oxygen batteries with alkyl-carbonate and ether based electrolytes. *Phys. Chem. Chem. Phys.* **2013**, *15*, 3623−3629.
(32) Hartmann, P.; Bender, C. L.; Sann, J.; Dürr, A. K.; Jansen, M.; Janek, J.; Adelhelm, P. A comprehensive study on the cell chemistry of the sodium superoxide (NaO_2) battery. *Phys. Chem. Chem. Phys.* **2013**, *15*, 11661−11672.
(33) Sun, Q.; Lin, X.; Yadegari, H.; Xiao, W.; Zhao, Y.; Adair, K. R.; Li, R.; Sun, X. Aligning the binder effect on sodium−air batteries. *J. Mater. Chem. A* **2018**, *6*, 1473−1484.
(34) Yadegari, H.; Franko, C. J.; Banis, M. N.; Sun, Q.; Li, R.; Goward, G. R.; Sun, X. How to Control the Discharge Products in Na−O_2 Cells: Direct Evidence toward the Role of Functional Groups at the Air Electrode Surface. *J. Phys. Chem. Lett.* **2017**, *8*, 4794−4800.
(35) Yadegari, H.; Norouzi Banis, M.; Lin, X.; Koo, A.; Li, R.; Sun, X. Revealing the Chemical Mechanism of NaO2 Decomposition by In Situ Raman Imaging. *Chem. Mater.* **2018**, *30*, 5156−5160.
(36) Black, R.; Shyamsunder, A.; Adeli, P.; Kundu, D.; Murphy, G. K.; Nazar, L. F. The Nature and Impact of Side Reactions in Glyme-based Sodium−Oxygen Batteries. *ChemSusChem* **2016**, *9*, 1795−1803.
(37) Sheng, C.; Yu, F.; Wu, Y.; Peng, Z.; Chen, Y. Disproportionation of sodium superoxide in Na-O_2 batteries. *Angew. Chem.* **2018**, *57*, 9906−9910.
(38) Cheon, J. Y.; Kim, K.; Sa, Y. J.; Sahgong, S. H.; Hong, Y.; Woo, J.; Yim, S.-D.; Jeong, H. Y.; Kim, Y.; Joo, S. H. Graphitic Nanoshell/Mesoporous Carbon Nanohybrids as Highly Efficient and Stable Bifunctional Oxygen Electrocatalysts for Rechargeable Aqueous Na−Air Batteries. *Adv. Energy Mater.* **2016**, *6*, 1501794.
(39) Khan, Z.; Senthilkumar, B.; Park, S. O.; Park, S.; Yang, J.; Lee, J. H.; Song, H.-K.; Kim, Y.; Kwak, S. K.; Ko, H. Carambola-shaped VO_2 nanostructures: a binder-free air electrode for an aqueous Na−air battery. *J. Mater. Chem. A* **2017**, *5*, 2037−2044.
(40) Ma, J.-L.; Yin, Y.-B.; Liu, T.; Zhang, X.-B.; Yan, J.-M.; Jiang, Q. Suppressing Sodium Dendrites by Multifunctional Polyvinylidene Fluoride (PVDF) Interlayers with Nonthrough Pores and High Flux/Affinity of Sodium Ions toward Long Cycle Life Sodium Oxygen-Batteries. *Adv. Funct. Mater.* **2018**, *28*, 1703931.
(41) Sun, B.; Li, P.; Zhang, J.; Wang, D.; Munroe, P.; Wang, C.; Notten, P. H. L. Dendrite-Free Sodium-Metal Anodes for High-Energy Sodium-Metal Batteries. *Adv. Mater.* **2018**, *30*, 1801334.
(42) Zhou, W.; Li, Y.; Xin, S.; Goodenough, J. B. Rechargeable Sodium All-Solid-State Battery. *ACS Cent. Sci.* **2017**, *3*, 52−57.
(43) Park, H.; Jung, K.; Nezafati, M.; Kim, C.-S.; Kang, B. Sodium Ion Diffusion in Nasicon ($Na_3Zr_2Si_2PO_{12}$) Solid Electrolytes: Effects of Excess Sodium. *ACS Appl. Mater. Interfaces* **2016**, *8*, 27814−27824.
(44) Wu, Y.; Qiu, X.; Liang, F.; Zhang, Q.; Koo, A.; Dai, Y.; Lei, Y.; Sun, X. A metal-organic framework-derived bifunctional catalyst for hybrid sodium-air batteries. *Appl. Catal., B* **2019**, *241*, 407−414.
(45) Medenbach, L.; Bender, C. L.; Haas, R.; Mogwitz, B.; Pompe, C.; Adelhelm, P.; Schröder, D.; Janek, J. Origins of Dendrite Formation in Sodium−Oxygen Batteries and Possible Countermeasures. *Energy Technol.* **2017**, *5*, 2265−2274.
(46) Sun, Q.; Liu, J.; Xiao, B.; Wang, B.; Banis, M.; Yadegari, H.; Adair, K. R.; Li, R.; Sun, X. Visualizing the Oxidation Mechanism and Morphological Evolution of the Cubic-Shaped Superoxide Discharge Product in Na−Air Batteries. *Adv. Funct. Mater.* **2019**, *29*, 1808332.
(47) Banis, M. N.; Yadegari, H.; Sun, Q.; Regier, T.; Boyko, T.; Zhou, J.; Yiu, Y. M.; Li, R.; Hu, Y.; Sham, T. K.; Sun, X.; Sun, X. Revealing the charge/discharge mechanism of Na-O_2 cells by in situ soft X-ray absorption spectroscopy. *Energy Environ. Sci.* **2018**, *11*, 2073−2077.
(48) Lutz, L.; Alves Dalla Corte, D.; Tang, M.; Salager, E.; Deschamps, M.; Grimaud, A.; Johnson, L.; Bruce, P. G.; Tarascon, J.-M. Role of Electrolyte Anions in the Na−O_2 Battery: Implications for NaO_2 Solvation and the Stability of the Sodium Solid Electrolyte Interphase in Glyme Ethers. *Chem. Mater.* **2017**, *29*, 6066−6075.

DOI: 10.1021/acs.chemmater.9b03266
Chem. Mater. 2019, 31, 9024−9031